Bull. Chem. Soc. Ethiop. **2026**, 40(10), 2221-2235.
DOI: https://dx.doi.org/10.4314/bcse.v40i10.12

ISSN 1011-3924
Printed in Ethiopia
Online ISSN 1726-801X


# EVALUATION OF NOVEL METAL-SCHIFF BASE COMPLEXES AS POTENT INHIBITORS AGAINST MICROBIOLOGICALLY INFLUENCED CORROSION (MIC)

Bushra Mohan[1*] and Naser Shaalan[2]

[1]Department of Chemistry, College of Science for Women, University of Baghdad, Baghdad, Iraq
[2]Department of Chemistry, College of Science for Women, University of Baghdad, Baghdad, Iraq

(Received January 14, 2026; Revised June 24, 2026; Accepted June 26, 2026)

**ABSTRACT**. Novel metallic complexes derived from a three coordinate hydrazine Schiff base ligand featuring an NNO electron donor system were prepared and characterized using FTIR, UV-Vis, ESI-MS, $^{1}$H, $^{13}$C-NMR, and CHN elemental analysis, supported by magnetic susceptibility and molar conductivity measurements. Structural studies confirmed a 2:1 molar ratio (L:M) for $Mn^{+2}$, $Co^{+2}$, $Ni^{+2}$, $Cu^{+2}$, and $Zn^{+2}$ complexes, while $Zr^{+4}$ exhibited a binuclear structure. Spectroscopic analysis revealed the ligand exists primarily in its enolic form. Based on the principle of structural similarity, an octahedral geometry was proposed for the divalent metal compounds and definitively confirmed for $Cu^{+2}$ via single-crystal X-ray diffraction (SC-XRD). To address microbial corrosion (MIC) challenges, the biological activity of these compounds ($10^{-3}$M) was evaluated as biocides against sulfate reducing bacteria (SRBs), fungal species (*Botrytis aclada* and *Absidia corymbifera*), and common pathogens. These included Gram positive bacteria (*Staphylococcus aureus*, *Streptococcus mutans*, and *Enterococcus faecalis*) and Gram negative bacteria (*Pseudomonas aeruginosa*). Notably, the Schiff base and its complexes exhibited significant antimicrobial activity, demonstrating performance comparable to synthetic chlorine based biopesticides.

**KEY WORDS**: Schiff base, Hydrazones, Microbiological corrosion, *Bacillus*, *Bortryis acaladia*, *Absidiomycete corimpifira*

## INTRODUCTION

Corrosion remains a significant industrial challenge, particularly in the oil and gas sector during production and transportation. Beyond the substantial economic burden, estimated by the National Association of Corrosion Engineers (NACE International) at approximately US$2.5 trillion globally [1], corrosion poses serious risks to structural integrity, security, and environmental stability [2, 3]. While various forms of corrosion exist, including galvanic and stress corrosion, microbiological corrosion (MIC) stands out as a particularly complex anaerobic problem [4]. In oxygen-free, sulfate-rich environments, sulfate-reducing bacteria (SRBs) play a key role by utilizing sulfates as the final electron acceptor, leading to the formation of corrosive iron sulfide [5]. To combat MIC corrosion, various strategies have been proposed, ranging from antioxidant coatings to corrosion-resistant alloys such as AISI 304 and 316 [6, 7]. However, research continues on highly efficient and environmentally compatible inhibitors. The chemistry of Schiff base bonds offers a strategic advantage in this field. These molecules, containing an azomethine group (C=N-) and negatively charged heteroatoms (nitrogen and oxygen), are characterized by high electron density and stable structures. These properties facilitate strong coordination with transition metal ions, forming stable chelated compounds capable of efficient adsorption onto metal surfaces [8]. Despite their potential, a clear research gap remains in the systematic study of tertiary coordinated hydrazonic (NNO) Schiff base compounds specifically designed to combat the dominant microbial strains in Iraqi oil environments. This study addresses this gap by

*Corresponding authors. E-mail: bushra.abd2305p@csw.uobaghdad.edu.iq

synthesizing a series of metal compounds derived from a novel NNO donor hydrazone bond. This research focuses on the synergistic effect between the bond structure and various metal centers (including tetravalent zirconium and divalent ions) to enhance inhibition efficacy. Using crude oil-contaminated water collected from the Al-Doura refinery in Baghdad, Iraq, this work evaluates the inhibitory effects of these newly synthesized compounds against sulfate-reducing bacteria and other pathogenic microorganisms. By bridging the gap between coordination chemistry and industrial application, this study aims to develop a robust, non-toxic protective barrier against the metabolic activities of corrosive microbes.

## EXPERIMENTAL

### *Materials and physical techniques*

All the basic chemicals used in the preparation of the amine, the bond, and their metal compounds were purchased from Merck. The solvents used were N, N-dimethylformamide (DMF) from CDH Central Pharmaceuticals and purified ethanol and methanol from BHD. Fourier transform infrared (FTIR) spectra were recorded in the 400-4000 $cm^{-1}$ Frequency range using a Perkin-Elmer spectrometer, while potassium bromide (KBr) and cesium iodide spectra were recorded in the 200-4000 $cm^{-1}$ frequency range for the compounds at room temperature. The analysis was performed in the Science Laboratory at the University of Baghdad. UV-Vis spectra were recorded using a Shimadzu UV-1800 spectrometer with two identical 10 mm quartz cells. The electron Transitions of the compounds. The masses of the ligands and their compounds were determined using electron spray ionization mass spectrometry (ESI-mass) with a Shimadzu LCMS 2010 and nuclear magnetic resonance spectrosCopy ($^{1}H$, $^{13}C$-NMR) with a Bruker instrument at 300 MHz. Weight loss was also monitored using thermogravimetric analysis (TGA) and its derivatives (DTG). Single-crystal analysis of the copper complex was performed using three-dimensional X-Ray diffraction. All these analyses were conducted at the laboratories of Shahid Beheshti University in Tehran, Iran.

### *Preparation*

#### *Preparation of the Schiff's base ligand (L1)*

In a 50 mL round-bottom flask, equal (1:1) proportions of 2-pyridine carboxaldehyde (0.372 g) (3.47 mmol) and 2-hydroxybenzohydrazide (0.528 g) (3.47 mmol) were condensed in 10 mL of absolute methanol at 40-50 °C for five hours, with the reaction completing and forming a white precipitate. The precipitate was filtered, washed with cold alcohol, dried, and its melting point was measured to be 225-227 °C [9, 10].

#### *Preparation of the Schiff bases L1 metal complexes*

In a 25 mL flat-bottomed flask, a Schiff base bond (0.15 g) was completely dissolved in 10 mL of a 50:50 v/v ethanol-methanol mixture. A few drops of dimethylformamide (DMF) were added to ensure complete dissolution. Appropriate metal salts, divalent metal chlorides ($Mn^{2+}$, $Co^{2+}$, $Ni^{2+}$, $Cu^{2+}$, and $Zn^{2+}$) or zirconium(IV) chloride were then added at a 1:2 molar ratio between the metal and the Ligand. The reaction mixture was stirred at 40-50 °C for 6 hours until a clear color change and precipitation occurred. The resulting solids were filtered, thoroughly washed with cold ethanol, and dried under vacuum (or at room temperature). Melting points were recorded, and the prepared compounds were stored for further characterization and analysis [11, 12].

*Isolation and identification of corrosive microorganisms*

Microbiological samples were collected from various locations within the Al-Doura oil refinery in Baghdad, Iraq, specifically from the internal surfaces of oil pipelines and the refinery's tenth pumping station, which exhibits localized corrosion. Microorganisms were isolated using water samples taken from the oil. To isolate the main microbial corrosion agents, the samples were cultured in specialized media. Sulfate-reducing bacteria were cultured using Postjet B medium under strict anaerobic conditions. For fungi and yeasts, potato dextrose agar (PDA) was used. Cultures were incubated at 37 °C for 48-72 hours.

Isolations were identified through a combination of morphological examination, Gram staining, and biochemical tests. A lead acetate test was also performed according to equation (1), and the test yielded a positive result with the precipitation of a black lead sulfide precipitate. This indicates the presence of hydrogen sulfide resulting from the anaerobic oxidation of sulfate-reducing bacteria. The corrosive bacterial isolate was identified as belonging to the genus Bacillus, while the fungal and yeast isolates were identified as belonging to the genera Botrytis and Absidia, two genera known for their ability to grow in hydrocarbon-rich environments and contribute to the decomposition of mineral substrates.

$$H_2S + Pb(CH_3COO)_2 \rightarrow PbS(s)\downarrow + 2CH_3COOH$$

black precipitate

Equation 1. Lead sulfate test for isolated bacteria.

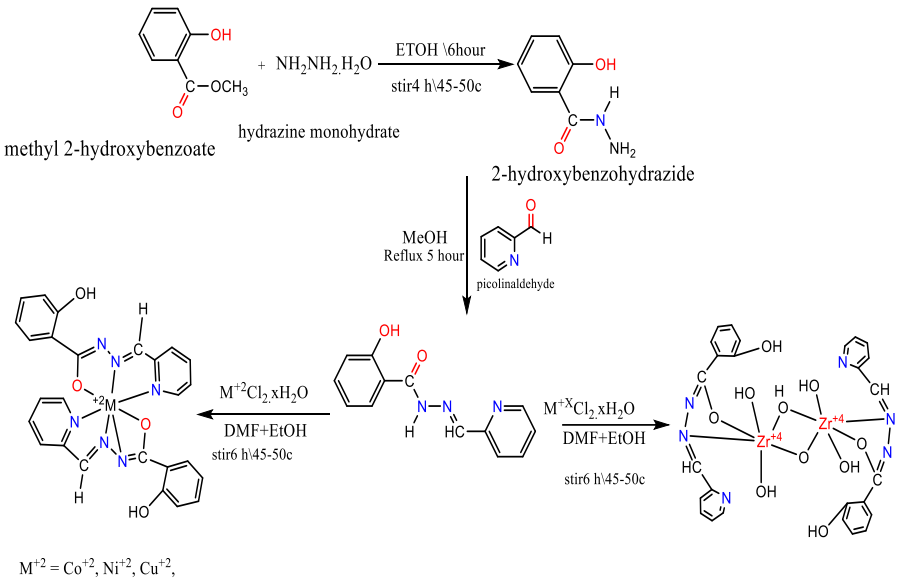


Scheme 1. Pathway of synthesis of metal-element complexes from Schiff bases.

Proposed formulas for complexes: $[Mn + 2(L)_2]Cl_2$ , $[Co(L)_2]$ $[Ni(L)_2]$ , $[Cu(L)_2.H_2O]$ , $[Zn Cl_2(L)_2]$, $[Zr_2 (L_1)_2(OH)_4 \mu\_(OH)_2]$.

## RESULTS AND DISCUSSION

*Elemental analysis*

The physical properties of the complexes with the ligand are listed in the following table

Table 1. Quantitative analysis of the elements and physical properties of the Schiff base and its metallic complexes.

| Formula suggestion | Color | M.P (°C) | Yield% | MWtg. $mol^{-1}$ | Elemental analysis found(Calc) | | | |
|---|---|---|---|---|---|---|---|---|
| | | | | | C | H | N | M |
| $C_{13}H_{11}N_3O_2$ | Creamy white | 225-227 | 89 | 241.245 | 63.97 (64.72) | 3.94 (4.60) | 17.64 (17.42) | ------- |
| $MnCl_2C_{26}H_{20}N_6O_4$ | Pale yellow | 240-243d | 82 | 608 | (51.33) | (3.65) | (13.82) | (9.03) |
| $C_{26}H_{20}N_6O_4Co$ | Dark Brown | 297d | 82 | 539 | 57.77 (57.89) | 3.46 (3.74) | 15.70 (15.58) | 11.2 (10.93) |
| $C_{26}H_{20}N_6O_4Ni$ | Brown | 297d | 93 | 539 | 57.92 (58.55) | 3.74 (3.53) | 15.59 (16.11) | (10.89) |
| $C_{26}H_{21}N_6O_5Cu$ | Dark Brown Crystals | >300 | 94 | 561.03 | (55,46) | (4.12) | (14.93) | (11.29) |
| | | *The formula of the compound was determined by three-dimensional XRD (single crystal). Its data was deposited with the Cambridge Centre for Crystal Structures (CCDC). | | | | | | |
| $Cl_2C_{26}H_{22}N_6O_4Zn$ | 0FF white | >300 | 75.7 | 619 | 50.47 | 3.58 | 13.58 | 10.57 |
| $O_2C_{26}H_{25}N_6O_8Zr$ | Gold | >300 | 92 | 764 | 39.73 (40.88) | 2.94 (3.30) | 10.64 (11) | (23.88) |

*Infrared spectroscopy*

FTIR spectroscopic analysis was utilized to confirm the successful synthesis of the Schiff base ligand (L1) and its corresponding metal complexes by monitoring the characteristic shifts in functional group frequencies. In the spectrum of the starting amine, the characteristic sharp bands appearing at 3319.49 $cm^{-1}$ and 3271.27 $cm^{-1}$ are assigned to the asymmetric and symmetric stretching vibrations of the N-H group, while the O-H stretching is observed at 3741.9 $cm^{-1}$ [13]. Upon condensation to form the free ligand (L1), distinct spectroscopic alterations were observed. The ligand spectrum exhibited key bands at 3462cm-1, 3242.24cm-1, 1629.85cm-1, and doublets at 1575cm-1,1544.98cm-1, which are securely attributed to O-H, N-H, C=O, and C=N azomethine stretching, respectively, along with the N-H bending at 1462.04cm-1. The noticeable lower-frequency shift of the O-H band in L1 3462 $cm^{-1}$ compared to the amine precursor is indicative of strong intra-intermolecular hydrogen bonding. Following complexation with the metal ions, significant modifications were observed, confirming the coordination of the ligand to the metal centers. Crucially, the carbonyl (C=O) band did not disappear but underwent a prominent negative shift to lower wavenumbers across the complexes (e.g., shifting from 1629.85$cm^{-1}$ in L1 to 1598.66 $cm^{-1}$ in ZrL1, demonstrating the direct involvement of the carbonyl oxygen in coordination (M-O). This shift is caused by the reduction of electron density within the {C=O} double bond due to the electron-withdrawing effect of the metal ion, which is further corroborated by the appearance of new metal-oxygen (M-O) bands in the (515-588) cm-1region.

Simultaneously, the azomethine (C=N) bands shifted to lower frequencies, and the disappearance of the N-H stretch in several complexes (such as CoL1, NiL1, CuL1, and ZrL1 suggests that the ligand undergoes enolization (enol hydrazone tautomerism) during coordination. This enolization is strongly favored by the electron-withdrawing effect of the adjacent pyridine ring, which enhances the acidity of the hydrazide proton, prompting the formation of the enolic structure. The key infrared vibrational bands for the Schiff base ligand and its metal complexes are summarized in Table 2.

Fourier transform infrared spectroscopy (FTIR) confirmed the binuclear fundamental structure by the appearance of characteristic bridge vibration frequencies (Zr-O-Zr, Zr-OH-Zr), which are completely absent in the free linker. The formation of the binuclear oxo, hydroxo core is directly attributed to the structural nature of the starting material, zirconyl chloride octahydrate ($ZrOCl_2.8H_2O$), which undergoes coordination while preserving the stable oxo, hydroxo bridging framework. This binuclear structure was verified and confirmed by elemental analysis (CHN), where experimental weight percentages showed accurate standard convergence with theoretical values specifically calculated for the binuclear structure.

Table 2. FT-IR spectral data (wave number ѵ)$cm^{-1}$ for ligand and its complexes.

| Comp Cod.. | ѵN-H stretch | ѵC=O | ѵC=N, C=N ring | ѵN-H Bending | C=C | ѵC-O | ѵM-N | ѵM-O | ѵO-H, and others |
|---|---|---|---|---|---|---|---|---|---|
| Amine | 3319.49 3271.27 | 1645.28 | ------ | 1587.4 | 1300 | ----- | ----- | ----- | 3741.9 |
| L1 | 3242.24 | 1629.85 | 1575, 1544.98 | 1462.04 | 1398 | ----- | ----- | ----- | 3462 |
| MnL1 | 3161.33 | 1612.49 | 1570.06 1516.05 | 1465.9 | 1442.7 | 1352.10 | 445.56 412.77 | 559.36 525.57 | 3300 |
| CoL1 | ----- | 1649.02 1602.74, | 1550.30 1510.16 | ------ | 1469.6 | 1301.85 | 447,45 | 540.03 | 3433.06 |
| NiL1 | ------ | 1622.02 | 1600.61, 1562.23 | ------ | 1457.7 | 1355.86, 1334.65 | 445 | 557.39 | 3496.70 |
| CuL1 | ----- | 1614, 1597. | 1552.7, 1551.8 | ---- | 1467.83 | 1397 | 476.42 424.34 | 588.29 528.50 | 3467 |
| ZnL1 | ------- | 1612.49 | 1573.91 | 1521.84 | 1489.05 | 1388.85 | 424.34 | 525.57 590.27 | 3427.5 |
| ZrL1 | ----- | 1598.66, | 1571.88 1541.02 | -------- | 1471.5 1450.3 | 1326.93 | 462.88, 439.74, | 515.89, | 3400, [Zr-O-Zr :1031-1056] |

*Mass spectrometry*

Electrospray ionization (ESI) mass spectrometry analysis was performed on the Schiff base ligand and two of its metal complexes (Ni(II) and Zr(IV)). The mass spectrum of the Schiff base ligand (L1) exhibited a peak at (m/z 241.95), which is consistent with its theoretically calculated molar mass (241 g/mol). The mass spectrum of the nickel complex showed a peak at m/z 540.80, matching the calculated mass of the complex and aligning with the quantitative, spectroscopic, and thermal analysis results. For the zirconium complex, the base peak was observed at m/z 241.95, attributed to the fragmented [L1+H+] ligand. Meanwhile, the complex itself exhibited a mass peak at m/z 809, which is close to the calculated mass of 764 g/mol. This mass difference ($\Delta m/z = 45$) can be attributed to the coordination or entrapment of lattice/coordinated water molecules, as zirconium(IV) complexes are highly hygroscopic due to the high charge density of the zirconium ion a finding that strongly agrees with the spectroscopic and thermal analytical data. Figures 1, 2, and 3 represent the ESI mass spectra of the Schiff base ligand, and its nickel and zirconium complexes, respectively [16, 17].

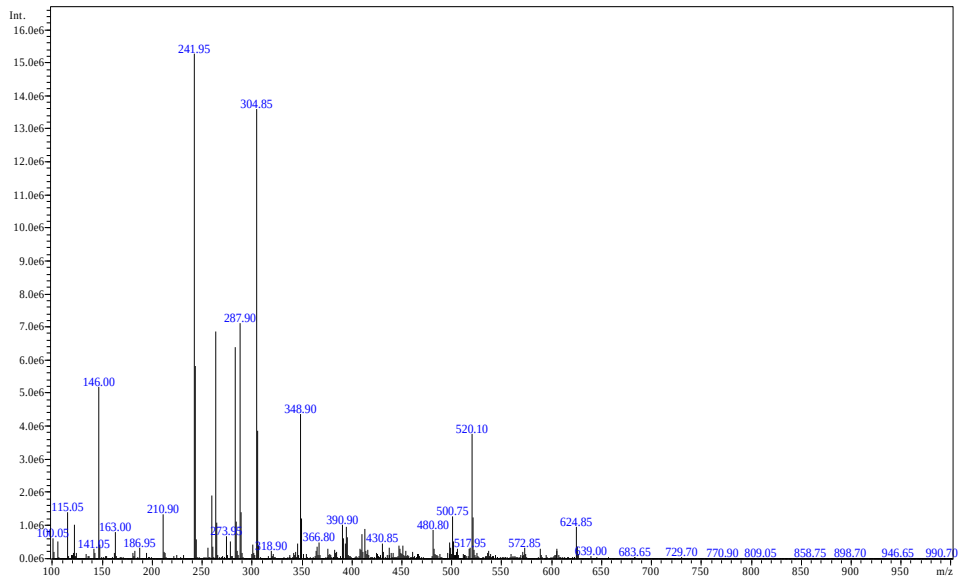


Figure 1. ESI-mass spectrum. for Schiff base ligand (L1).

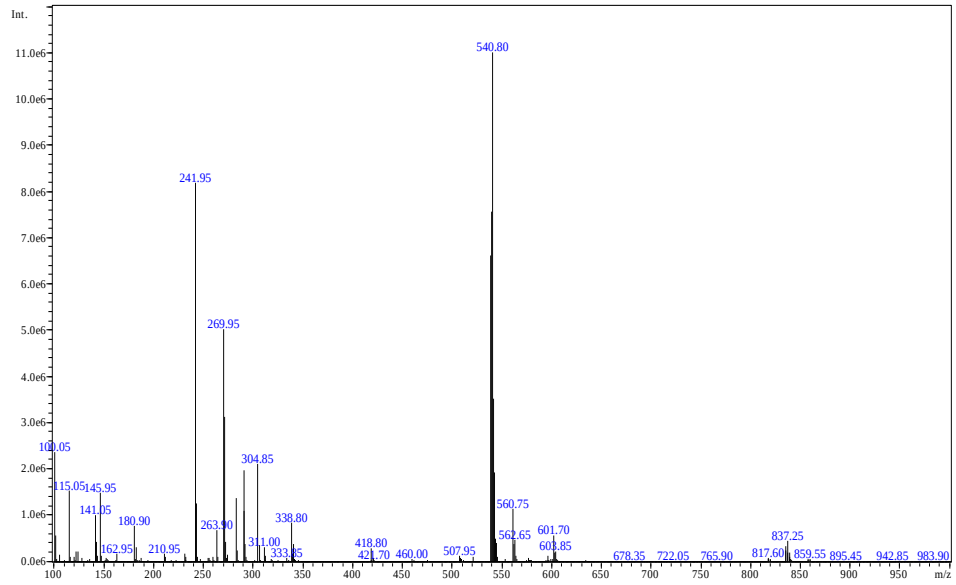


Figure 2. ESI-Mass spectrum. for NiL1 complex.

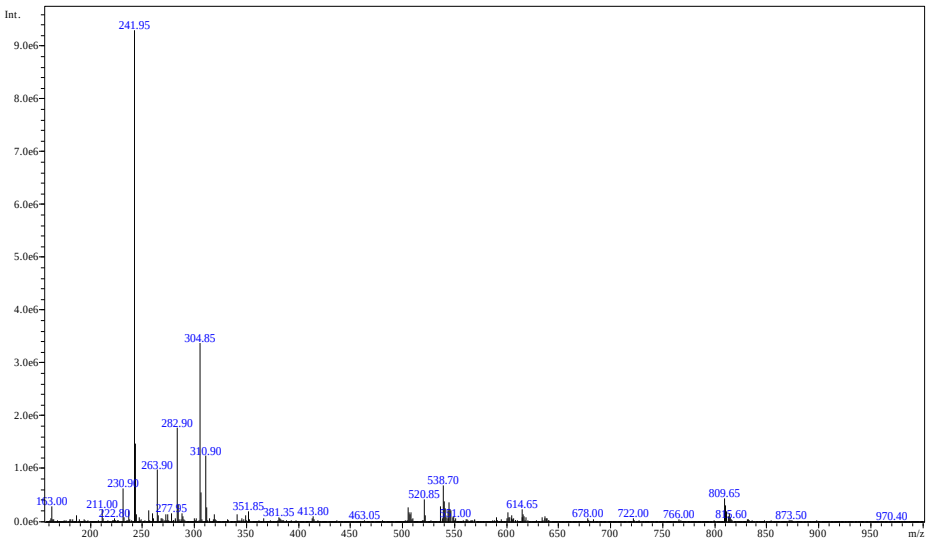


Figure 3. ESI-Mass spectrum. for ZrL1 complex.

*Electronic spectroscopy*

The ligand spectrum showed a range of bands, three of which were prominent in the ultraviolet region. These bands are attributed to (n→π*) transitions resulting from the presence of heteroatoms with unpaired electrons. The spectra of the colored coordination complexes also showed a range of new bands in both the ultraviolet and visible regions. The spectra of complexes that retained the ligand's color were distinguished in the ultraviolet region, due to the saturation of the d orbital. These complexes include zinc-molybdenum complexes. The manganese complex showed two bands (550, 600) nm attributed to two transitions (6A1g→4T1g, 6A1g→4T2g) and a magnetic moment of 3.619 B, consistent with an octahedral shape. Brown cobalt complexes exhibited several bands (674,608,406 and 361)nm attributed to the 4T1g(F)→4T2g(F), 4T1g(F)→4T1g(P), and 4T1g(F)→4A2g(F) transitions, and a magnetic moment of 2.4 Bm.( that these complexes undergo a Spin Crossover (SCO) phenomenon or stabilize in specific spin states due to the ligand field strength of the novel Schiff base.) [20, 21]. Nickel complexes exhibited several bands (790, 670, and 454)nm attributed to the {3A2g(F)→3T2g(F), ѵ2=3A2g(F)→3T1g(F), ѵ1=3A2g(F)→3T1g(p)} transitions, and a magnetic moment of 2.4 Bm. The copper complexes exhibited three bands in the visible light region, attributed to the transitions (ѵ=2B1g→2A1g, ѵ=2B1g→2B2g, ѵ=2B1g→2E1g), appearing as a single broad peak due to the convergence and overlap of these bands. This broad peak was also observed to shift towards a longer wavelength, attributed to the distortion of the octahedral crystal structure, [18, 19] as demonstrated by three-dimensional X-ray diffraction. The zinc complex, on the other hand, exhibited transitions in the ultraviolet region (366, 278, 233) nm, attributed to (π→π*, n→π*, CTLM). As for the zirconium compound, which exhibited a magnetic moment of zero, it had three charge transitions in the ultraviolet region and the beginning of the visible region, located at (541, 415, 379, 360, 274) nm. These transitions are represented by (CTLM, n→π*, π→π), respectively. The yellow color of the compound is attributed to the charge transitions that occurred at the beginning of the visible region [22, 23].

*$^{1}$H-NMR, $^{13}$C-NMR spectra*

NMR results for Schiff base L1 and its metal complexes revealed a set of signals in DMSO, which we will discuss in detail. The proton nuclear magnetic resonance ($^{1}$H-NMR) spectrum of the L$^{1}$ Schiff bond in $d_6$ dimethyl sulfoxide showed prominent single signals at 12.04 and 11.71 ppm, attributed to the protons of the phenolic hydroxyl (-OH) and amine (-NH) groups, respectively. The aromatic ring protons of phenyl and pyridine appeared as multiple signals in the range of 6.98-8.63 ppm [24]. For the nickel(II) complex, the resonant signals of the phenolic hydroxyl (OH) and amine (-NH) groups shifted to 12.24 and 10.18 ppm, while the aromatic ring protons appeared in the range of 6.48-8.62 ppm. It is noteworthy that the clear and sharp proton nuclear magnetic resonance ($^{1}$H-NMR) spectra of nickel(II), which initially appeared inconsistent with its solid-state magnetic moment (2.40 B.M), are scientifically justified by the existence of a dynamic equilibrium between the octahedral (paramagnetic) and square-planar (diamagnetic) structures in solution. These sharp resonances arise primarily from the diamagnetic square-planar region, devoid of paramagnetic relaxation amplitude [25]. The bimetallic zirconium(IV) compound exhibited signals in the low magnetic field at 12.01- 13.63 ppm, corresponding to uncoordinated hydroxyl groups and coordinated water molecules. The protons of the phenyl and pyridine aromatic rings shifted to the 6.57-8.93 ppm region. The multiplicity and splitting of these signals strongly support the formation of a binuclear structure, as confirmed by elemental analyses and mass spectrometry. In addition, the single signal at 3.16 ppm is attributed to residual moisture in the DMSO-$d_6$ solvent. The weak signals observed in the aliphatic region (1.0-1.3 ppm) of both compounds do not belong to the Schiff base structure; rather, they are definitively attributed to trace background impurities, including residual washing solvents (ethanol/ethyl acetate) and vacuum silicone grease from glass vessel joints. Figure 4) shows the proton signals of the ligand.

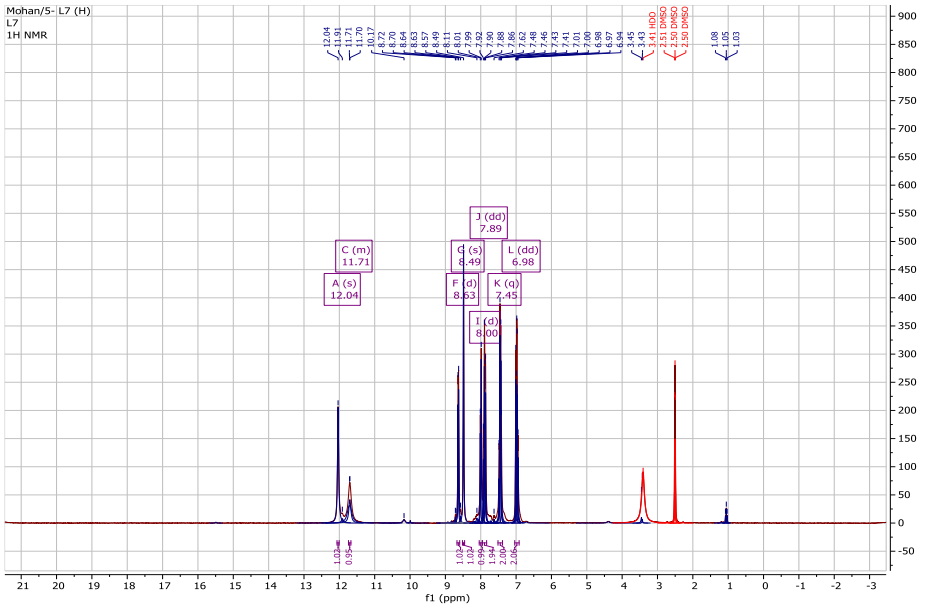


Figure 4. Shows the proton signals of the ligand L1.

*$^{13}$C-NMR*

The carbon-13 nuclear magnetic resonance ($^{13}$C-NMR) spectrum of the $L^{-1}$ Schiff base ligand showed characteristic signals for carbonyl (C=O) and azomethine (C=N) carbonates at 165.0 and 159.0 ppm, respectively. Aromatic and heterocyclic carbonates (C=C, C-C, and C-N) were segregated within the 116.0-153.0 ppm range [26]. For the nickel(II) compound, the complete disappearance of the carbonyl (C=O) signal, accompanied by the appearance of a new resonance at 175.0 ppm, confirms the association of the hydrazide moiety in its enolic form (-C=N-C-O-M). The remaining aromatic carbon atoms were observed at 139.9 and 116.0 ppm, with some signals being limited due to the compound's low solubility [27]. The binuclear zirconium(IV) compound exhibited signals shifted toward the lower magnetic field at 175.46 ppm, attributed to the phenolic carbon atom bearing the hydroxyl group (-OH), confirming its participation in the symmetry. Azomethine (C=N) carbon atoms appeared as multiple signals around 159.45-159.96 ppm, while aromatic (C=C) and C-N carbon atoms appeared at 114.31-151.79 ppm and 127.52-128.95 ppm, respectively [28]. These cleavage patterns support the asymmetric environment within the proposed multinuclear framework.

*Thermal analysis TGA and DTG*

Thermogravimetric analysis (TGA) and differential thermogravimetric analysis (DTA) curves for the Schiff base and its metal compounds show that the bond undergoes thermal decomposition from room temperature to 800 ℃. For this bond, the TGA curve in Figure 5 indicates three stages of weight loss. The first stage involved a 2.70% loss of the total bond mass between 50 and 120 °C. This range is typically associated with the loss of volatile substances, moisture, or impurities, including solvent interference. In the second stage, approximately 41.24% of the bond mass was lost between 120 and 400 °C. This mass is equivalent to about 99.488 g/mol, from which the fraction (C6H6N2) was derived. In the third stage, 56.22% was lost, equivalent to 135.62 g/mol, from which the fraction (C7H5NO2) was derived. The remaining mass was 0.1%. This percentage is very small and does not represent a portion of the compound; it is likely due to impurities. The two compounds selected for this analysis, nickel and zirconium, underwent the weight-loss stages shown in the table: three stages for each compound [29].

The thermogravimetric analysis (TGA) curve in Figure 6 shows that the first two weight-loss stages in the nickel compound involved very small mass losses, which may be due to volatile substances, chemical reaction products, or may not be part of the compound's total mass. The weight-loss stages of the compound are thought to have begun after 300 ℃, with a loss of 30.88% (166.543 g/mol), and it has been suggested that this loss is due to (C12NH9). The next stage involved a loss of 60.17%, equivalent to 324.417 g/mol, and the loss of (C10H11N5NiO4) has been suggested. Thus, the remaining mass of the compound was 7.17%, equivalent to 48.2 g/mol. This weight corresponds to four carbon atoms. The thermogravimetric (TGA) curve in Figure 7 shows that the weight loss of zirconium occurred in three stages. The first stage involved a 7.23% weight loss between 50 and 140 °C, corresponding to a mass loss of 58.2 g/mol, attributed to the proposed loss of ($N_2COH_2$). The second stage involved a 4.94% weight loss between 140 and 280 °C, equivalent to a mass loss of 39.787 g/mol, corresponding to the proposed loss of the fraction (N2C). The third stage involved a 61% weight loss between 280 and 750 °C, corresponding to a molar mass of 491.05 g/mol, which was attributed to the loss of the fragment ($C_{24}Cl_4H_{16}O$). The remaining mass from the thermal decomposition of zirconium was 26.83%, equivalent to 215.98 g/mol, and is thought to be zirconium oxide ($ZrO_2$) [30, 31].

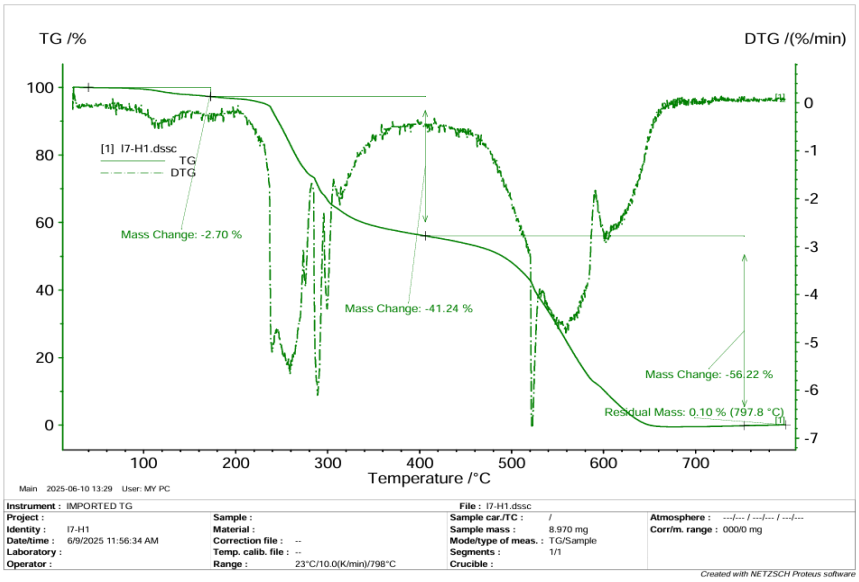


Figure 5. The TGA\DTG analysis of the Schiff base.

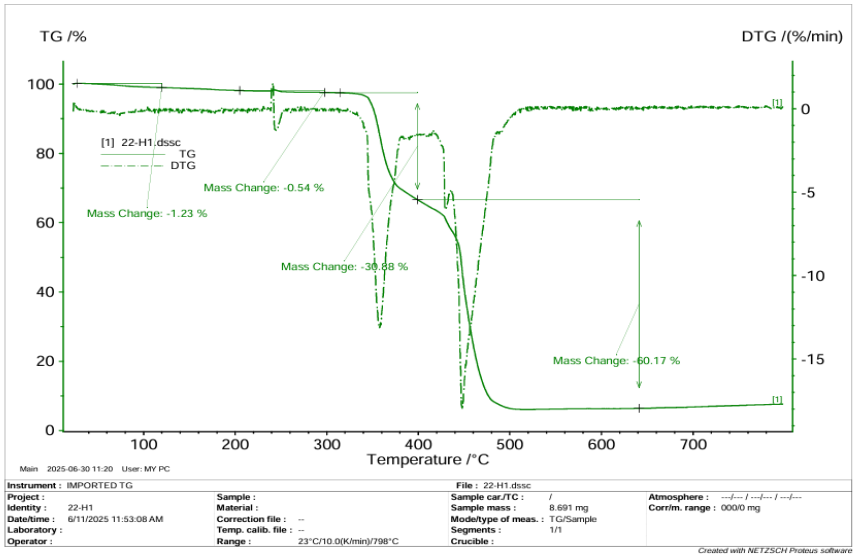


Figure 6. the TGA\DTG analysis of the NiL1 complex.

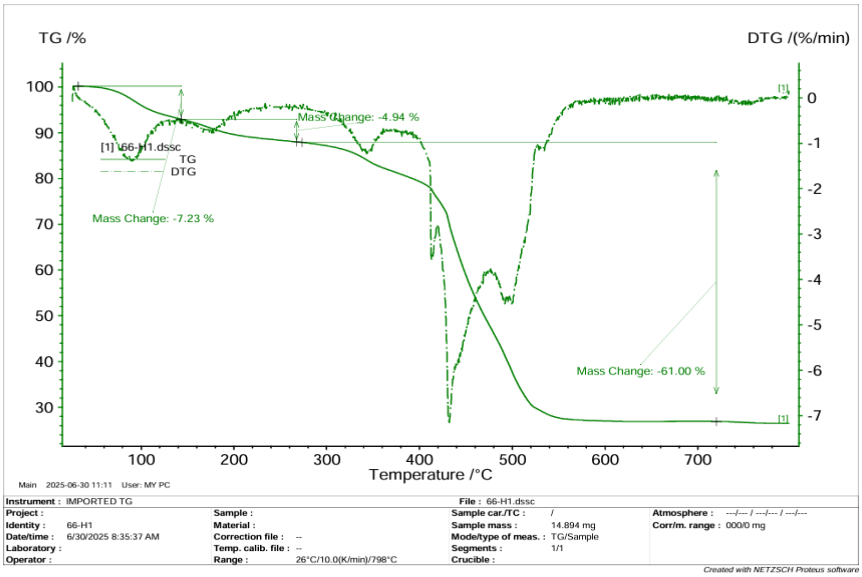


Figure 7. The TGA\DTG analysis of the ZrL1 complex.

*Biological activity and biological inhibition of corrosion*

Bacterial and fungal species were isolated and classified from oil-contaminated water collected from the target site. To evaluate the antimicrobial efficacy against these biologically corrosive isolates, solutions of the synthesized Schiff base (L1) and its complexes were prepared at a concentration of 0.001 M. The corrosive isolates included a sulfate-reducing bacterium, Bacillus sp. Y2, and two fungal strains, *Botrytis sp.* and *Absidia corymbifera* [32]. For taxonomy verification, although molecular sequencing for Bacillus sp. Y2 was unavailable due to local infrastructural limitations. The isolate was systematically identified through comprehensive phenotypic and biochemical profiling based on Bergey's Manual of Systematic Bacteriology [33], including Gram staining, endospore verification, catalase/oxidase testing, and carbohydrate fermentation profiles. For comparative biological analysis, four pathogenic strains were tested: Gram-positive (*Staphylococcus aureus* [34], *Streptococcus mutans*, and *Enterococcus faecalis*) and Gram-negative (*Pseudomonas aeruginosa*). A commercial chlorine compound used at the industrial site and standard antibiotics served as reference controls. Table 2 summarizes the inhibition zones, highlighting the enhanced antibacterial and antifungal properties of the Schiff base (L1) and its metal complexes [35]. Standard controls included Chlorhexidine, Kanamycin, and Ciprofloxacin for bacteria, and Nystatin, Fenhexamid (0.045% v/v), and Voriconazole (>16 g/mL) for fungi [36-40] (where N.A = No Activity).

Table 2. Zones of inhibition showing antibacterial activities of Schiff base(L1) and its complexes against bacteria and fungi.

| Comp. | *Enterobacter faecalis (ve+)* | *Streptococcus mutans (ve+)* | *Pseudomonas aeruginosa (ve-)* | *Staphylococcus aureus (ve+)* | *Y2 (Bacillus)* |
|---|---|---|---|---|---|
| Ligad L | 4 | 20 | 11 | 20 | 16 |
| Co L | 5 | 20 | 11 | 10 | 5 |
| NiL | 4 | 20 | 10 | 10 | 3 |
| CuL | 6 | 18 | 13 | 15 | 8 |
| ZrL | 1 | 3 | 10 | 2 | 5 |
| DMF | ---- | ----- | ---- | ----- | ---- |
| Chlorine 7%., 5% | | | | | 15. 7 |
| Chlorhexidine.[a] | 3.69* | 0.46* | ------ | ------ | ------ |
| Kanamycin B[b] | ----- | ------ | ------ | 1.56** | ------ |
| CIP:Ciprofloxacin.[c] | ------ | ------ | 0.12*** | 0.12*** | ------ |
| Nystatin[d] | | | | | N.A. |
| Fungi | L7(8) | Zr (9) | Ni (10) | Zn (11) | Co(12) |
| *Bortryis* . | ++ | ++ | - | - | - |
| *Absidia* | + | + | + | + | + |

## CONCLUSIONS

In conclusion, a novel Schiff base ligand (L1) was successfully synthesized from 2-hydroxybenzohydrazide and 2-pyridinecarbaldehyde and systematically coordinated with a variety of transition-metal ions. The structural flexibility of the ligand allows for distinct coordination patterns determined by the nature and oxidation state of the metal center. Comprehensive spectroscopic, thermal, magnetic, and conductivity evaluations confirmed the proposed geometries and determined the composition of $[M(L1)_2Cl_2]$ (where M = Mn(II), Co(II), Ni(II), $[Cu(L1)2H_2O]$, $[ZnCl_2(L1)_2]$, and the unique dinuclear framework $[Zr_2O_2(L1)_2(OH)_4]$. The distorted octahedral geometry and covalent nature of the copper compound were definitively verified using X-ray diffraction on a single crystal, and the data were deposited in the Cambridge Crystal Data Center (CCDC No. 2495340). Biologically, the synthesized compounds demonstrated exceptional antimicrobial activity at a concentration of $10^{-3}$ M against highly biofilm-forming and microbially corrosive microbial isolates. Notably, the newly developed compounds exhibited significantly higher bactericidal efficacy than currently used commercial chlorine-based treatments, making them highly effective alternative biocides for mitigating microbial corrosion in industrial oil refineries.

## ACKNOWLEDGMENT

The authors express their thanks and appreciation to Shahid Beheshti University for technical support, and extend their thanks to the engineering and technical staff at the Dora refinery.

## REFERENCE

1. Hassan, A.; Numin, M.S.; Jumbri, K.; Kee, K.E.; Borhan, N. Review on the recent development of fatty hydrazide as corrosion inhibitor in acidic medium: experimental and theoretical approaches. *Met. Sci. J.* **2022**, 12, 2-21.

2. Benkhaya, S.; M'rabet, S.; El Harfi, A. Classifications, properties, recent synthesis and applications of azo dyes. *Heliyon* **2020**, 6, 1-21.
3. Czaban, M. Aircraft corrosion – review of corrosion processes and its effects in selected cases. *Fatigue Aircraft Struct*. **2018**, 2018, 10, 5-20.
4. Enning D.; Garrelfs J. Corrosion of iron by sulfate-reducing bacteria: New views of an old problem. *Appl. Environ. Microbiol*. **2014**, 80, 1226-1236.
5. Faili, N.T.; Burghal, K.S. Preparation and evaluation of waste ground tyre rubber as antioxidant, antibacterial agent and corrosion inhibitor for N80 steel in 0.1N $H_3PO_4$. *Baghdad Sci. J.* **2024**, 21, 2319-2330.
6. Husseini, M.; Latief, B.H.; Khudhair, N.A.; Huseeni, M.D.; Al-Saadi, F.A. Investigation of corrosion inhibition of carbon steel by using natural Iraqi plum tree gum in a saline medium. *Iraqi J. Sci*. **2024**, 65, 5349-5356.
7. Pospieszna-Markiewicz, I.; Fik-Jaskółka, M.A.; Hnatejko, Z.; Patroniak, V.; Kubicki, M. Synthesis and characterization of lanthanide metal ion complexes of new polydentate hydrazone Schiff base ligand. *Molecules* **2022**, 27, 2-14.
8. Ahamed, L.S.; Al-Rekabi, Z.G. Synthesis of aryl hydrazone derivatives for α-naphthalide and benzothiazolide. *Baghdad Sci. J.* **2025**, 7, 1-7.
9. Munir, R.; Javid, N.; Zia-ur-Rehman, M.; Zaheer, M.; Huma, R.; Roohi, A.; Athar, M.M. Synthesis of novel N-acylhydrazones and their C–N/N–N bond conformational characterization by NMR spectroscopy. *Molecules* **2021**, 26, 2-18.
10. Sastri, V.S. *Types of corrosion inhibitor for managing corrosion in underground pipelines. In: Underground Pipeline Corrosion: Detection, Analysis and Prevention*; *Woodhead Publishing Ltd.: Cambridge*, **2014**; p 166-211.
11. Hussain, E.M. Synthesis and antibacterial evaluation for some new Schiff bases derived from p-aminoacetanilide. *Baghdad Sci. J.* **2023**, 20, 2455-2466.
12. Mohan, B.; Shaalan, N. Synthesis, spectroscopic and biological activity study for new complexes of some metal ions with Schiff bases derived from 2-hydroxy naphthaldehyde with 2-amine benzhydrazide. *Ibn Al-Haitham J. Pure Appl. Sci*. **2023**, 36, 208-224.
13. Raczuk, E.; Dmochowska, B.; Samaszko-Fiertek, J.; Madaj, J. Different Schiff bases: Structure, importance and classification. *Molecules* **2022**, 27, 2-24.
14. Bhaskar, R.S.; Ladole, C.A.; Salunkhe, N.G.; Aswar, A.S. Synthesis, characterization and biological studies of some transition metal complexes with pyrazine Schiff base hydrazone ligand. *Jordan J. Chem*. **2020**, 15, 61-72.
15. May, A.; Ghada, A. Ability of *Staphylococcus epidermidis* and *Escherichia coli* to eliminate cadmium, lead and copper from Tigris river in Mosul city. *Baghdad Sci. J*. **2025**, 22, 2612-2618.
16. Preethi, V.; Vijukumar, V.G.; AnilaRaj, S.; Vidya, V.G. Synthesis, characterization, DFT studies and evaluation of the potential anti-tumour activity of nicotinic hydrazide based Schiff base using in vitro and molecular docking techniques. *Heliyon* **2024**, 10, e29689.
17. McIndoe, J.S.; Vikse, K.L. Assigning the ESI mass spectra of organometallic and coordination compounds. *J. Mass Spectrom*. **2019**, 54, 466-479.
18. Markert, C.; Thinius, M.; Lehmann, L.; Heintz, C.; Stappert, F.; Wissdorf, W.; Hendrik, K.; Thorsten, B.; Bradley, B.; Thomas, R. Observation of charged droplets from electrospray ionization (ESI) plumes in API mass spectrometers. *Anal. Bioanal. Chem.* **2021**, 413, 5587-5600.
19. Alias, M.; Omran, S. Mixed ligand complexes of quinoline-2-carboxylic acid and 4,4′-dimethyl-2,2′-bipyridyl with V(IV), Cr(III), Rh(III), Cd(II) and Pt(IV). *Baghdad Sci. J*. **2014**, 11, 1180-1190.
20. Gütlich, P., Goodwin, H.A. (Eds.). *Spin Crossover in Transition Metal Compounds I*, 1st ed.; Springer-Verlag: Berlin, Germany; **2004**; pp. 1-55.

21. Gera, E.; Vignesh, K.R. A systematic comparison of density functional methods for determining spin-state energy gaps and spin transition temperature of spin crossover complexes. *RSC Advances*, **2026**, 16, 2241-2254
22. Al-Hakimi, A.N.; Alminderej, F.; Aroua, L.; Alhag, S.K.; Alfaifi, M.Y.; Samir, O.M.; Mahyoub, J.A.; Elbehairi, S.E.I.; Alnafisah, A. Design, synthesis and characterization of zirconium(IV), cadmium(II) and iron(III) complexes derived from Schiff base 2-aminomethylbenzimidazole and 2-hydroxynaphthaldehyde and evaluation of their biological activity. *Arab. J. Chem*. **2020**, 13, 7378-7389.
23. Hijazi, A.K.; Taha, Z.A.; Issa, D.K.; Alshare, H.M.; Al-Momani, W.M.; Elrashidi, A. Synthesis, characterization and catalytic/antimicrobial activities of some transition metal complexes derived from 2-fluoro-N-((2-hydroxyphenyl)methylene)benzohydrazide. *Molecules* **2024**, 29, 5758.
24. Komyha, E.M.; Mahmoud, W.H.; Hosny, W.M.; El-Sherif, A.A. Design, structural characterization, molecular docking and biomedical applications of hydrazone-based Schiff base metal complexes. *Egypt. J. Chem.* **2023**, 66, 121930.
25. Kostova, I.; Manolov, I.; Karaivanova, M. Synthesis, physicochemical characterization and cytotoxic screening of new zirconium complexes with coumarin derivatives. *Arch. Pharm. (Weinheim)* **2001**, 334, 157-162.
26. Shaalan, N.; Hussein, N.A. Synthesis, characterization, biological activity and thermal studies of new metal ion complexes with Schiff base derived from dimedone and 2-hydroxybenzohydrazide. *Bull. Chem. Soc. Ethiop*. **2025**, 39, 2271-2280.
27. Asiri, S.; Kassem, M.A.; Eltaher, M.A.; Saad, K.M. Novel coordination compounds based on copper complexes with newly synthesized Schiff bases and azo dyes as sensitizers for dye-sensitized solar cells: spectral and electrochemical studies. *Int. J. Electrochem. Sci*. **2020**, 15, 6508-6521.
28. Yadav, P.; Sarkar, A.; Singh, A.; Singh, A.K.; Nirala, R.K.; Naqvi, I.; Verma, D.; Jit, B.P.; Jaiswal, M. Spectral characterization and biological activities of Schiff base metal complexes. *Corros. Prot*. **2023**, 51, 832-849.
29. Al-Redha, H.M.A.; Ali, S.H.; Mohammed, S.S. Syntheses, structures and biological activity of some Schiff base metal complexes. *Baghdad Sci. J*. **2022**, 19, 704.
30. Senila, L.; Hoaghia, A.; Moldovan, A.; Török, I.A.; Kovacs, D.; Simedru, D. The potential application of natural clinoptilolite-rich zeolite as support for bacterial community formation for wastewater treatment. *Materials* **2022**, 15, 3685.
31. Dhedan, R.M.; Awaad, S.H.; Fadhl, S.N. Synthesis and characterization of new acrylamide derivatives and study of their antibacterial activity. *Baghdad Sci. J.* ***2024***, 22, 361-370.
32. Shi, X.; Zhang, R.; Sand, W.; Mathivanan, K.; Zhang, Y.; Wang, N. Comprehensive review on the use of biocides in microbiologically influenced corrosion. *Microorganisms* **2023**, 11, 2194.
33. Whitman, W.B.; Goodfellow, M.; Kampfer, P.; Busse, H.J.; Trujillo, M.E.; Ludwig, W.; Suzuki, K.I. *Bergey's Manual of Systematic Bacteriology*, 2nd ed.; Springer: New York, NY, USA, **2012.**
34. Al-Hassani, M.J.A.; Al-Muhammadi, R.A.M. Synthesis, structural characterization and antimicrobial assessment of transition metal complexes derived from a Mannich base of 5-chloro-2-mercapto-oxazole. *Bull. Chem. Soc. Ethiop*. **2026**, 40, 199-210.
35. Zhang, F.; Wen, Q.; Wang, S.F.; Karim, S.B.; Yang, Y.S.; Liu, J.J. Design, synthesis and antibacterial activities of 5-(pyrazin-2-yl)-4H-1,2,4-triazole-3-thiol derivatives containing Schiff base formation as FabH inhibitors. Bioorg. *Med. Chem. Lett*. **2014**, 24, 90-95.
36. Sampiron, E.G.; Costacurta, G.F.; Baldin, V.P.; Almeida, A.L.; Ieque, A.L.; Santos, N.C.S. Hydrazone, benzohydrazones and isoniazid-acylhydrazones as potential antituberculosis agents. *Future Microbiol*. **2019**, 14, 981-994.

37. Omidi, S.; Kakanejadifard, A. A review on biological activities of Schiff base, hydrazone and oxime derivatives of curcumin. *RSC Adv*. **2020**, 10, 30186-30202.
38. Chau, A.S.; Chen, G.; McNicholas, P.M.; Mann, P.A. Molecular basis for enhanced activity of posaconazole against *Absidia corymbifera* and *Rhizopus oryzae*. *Antimicrob. Agents Chemother*. **2006**, 50, 3917-3919.
39. Carreño, A.; Páez-Hernández, D.; Cruz-López, P. Structural characterization, DFT calculation, NCI, scan-rate analysis and antifungal activity against Botrytis cinerea of (E)-2-{[(2-aminopyridin-2-yl)imino]methyl}-4,6-di-tert-butylphenol (pyridine Schiff base). *Molecules* **2021**, 26, 167-186.
40. Rupa, S.A.; Moni, M.R.; Patwary, M.A.M.; Mahmud, M.M.; Haque, M.A.; Uddin, J. Synthesis of novel tritopic hydrazone ligands: spectroscopy, biological activity, DFT and molecular docking studies. *Molecules* **2022**, 27, 1656.